Published in final edited form as:
Magn Reson Med. 2010 June ; 63(6): 1548–1556. doi:10.1002/mrm.22329.

Combined Arterial Spin Label and Dynamic Susceptibility Contrast Measurement of Cerebral Blood Flow

Greg Zaharchuk[1,*], **Matus Straka**[1], **Michael P. Marks**[1], **Gregory W. Albers**[2], **Michael E. Moseley**[1], and **Roland Bammer**[1]

[1] Department of Radiology, Stanford University, Stanford, California, USA

[2] Stanford Stroke Center, Department of Neurology and Neurological Sciences, Stanford University Medical Center, Stanford, CA, USA

Abstract

Dynamic susceptibility contrast (DSC) and arterial spin labeling (ASL) are both used to measure cerebral blood flow (CBF), but neither technique is ideal. Absolute DSC-CBF quantitation is challenging due to many uncertainties, including partial-volume errors and nonlinear contrast relaxivity. ASL can measure quantitative CBF in regions with rapidly arriving flow, but CBF is underestimated in regions with delayed arrival. To address both problems, we have derived a patient-specific correction factor, the ratio of ASL- and DSC-CBF, calculated only in short-arrival-time regions (as determined by the DSC-based normalized bolus arrival time [Tmax]). We have compared the combined CBF method to gold-standard xenon CT in 20 patients with cerebrovascular disease, using a range of Tmax threshold levels. Combined ASL and DSC CBF demonstrated quantitative accuracy as good as the ASL technique but with improved correlation in voxels with long Tmax. The ratio of MRI-based CBF to xenon CT CBF (coefficient of variation) was 90 ± 30% (33%) for combined ASL and DSC CBF, 43 ± 21% (47%) for DSC, and 91 ± 31% (34%) for ASL (Tmax threshold 3 sec). These findings suggest that combining ASL and DSC perfusion measurements improves quantitative CBF measurements in patients with cerebrovascular disease.

Keywords

magnetic resonance imaging; perfusion; computed tomography; xenon CT; cerebral blood flow; quantitative

Bolus dynamic susceptibility contrast (DSC) perfusion-weighted imaging (PWI) and arterial spin labeling (ASL) are two methods of measuring cerebral blood flow (CBF) using MRI, each with different strengths and weaknesses (1–3). ASL CBF levels are reliable in regions with rapidly arriving flow but suffer from reduced signal-to-noise ratio (SNR), CBF underestimation, and artifacts in regions with long arterial arrival times (4–7). In theory, DSC-based CBF measurements are unaffected by long arrival times if Fourier-based or delay-invariant block-circulant singular value decomposition deconvolution methods are used (8–10). However, absolute quantitation is challenging for many reasons, including uncertainties regarding the arterial input function (AIF) partial-volume amount, the effect of vessel orientation on contrast relaxivity, the nonlinear relationship between transverse relaxivity and contrast concentration, clipping of AIF signal due to high tracer concentrations, and

*Correspondence to: Greg Zaharchuk, M.D., Ph.D.,1201 Welch Rd., PS-04, Stanford University Medical Center, Mailcode 5488, Stanford, CA 94305-5488. gregz@stanford.edu.

Additional Supporting Information may be found in the online version of this article.

susceptibility-based voxel shifting (11–15). For these reasons, both techniques have yet to be fully embraced by the neuroimaging community for evaluating patients with cerebrovascular disease.

This study describes a calibration method that uses ASL CBF measurements in regions with short transit delays (as measured by the AIF-normalized time to peak of the residue function [Tmax]) to provide a patient-specific correction factor (CF) for DSC CBF measurements. We have termed this method "*c*ombined *A*SL and *D*SC *CBF*," or CAD-CBF. We hypothesize that in patients with cerebrovascular disease, the CAD-CBF method will have less bias and more precision with respect to a gold-standard CBF method. We also hypothesize that application of such a CF will improve CBF measurements in long arterial arrival time regions compared with ASL. To test this, we have evaluated 20 patients with known cerebrovascular disease who received xenon CT (xeCT) and MR perfusion imaging. xeCT is a gold-standard perfusion measurement that uses a diffusible tracer (xenon gas) that is inhaled by the patient and that permits CBF measurement using the autoradiographic ("Kety-Schmidt") method (16,17).

MATERIALS AND METHODS

Patient Population

The study was approved by the institutional review board and was Health Insurance Portability and Accountability Act (HIPAA) compliant. Patients were enrolled if they had symptoms concerning for cerebral ischemia (acute, subacute, or chronic) or transient ischemic attack and were willing to undergo the xeCT CBF study. To be included in the study, the stable xeCT and MRI studies had to occur within a 48-h period.

Twenty patients met the inclusion criteria (11 men, nine women; mean age 53 years; range 25–74 years). Their clinical indications were as follows: 13 moyamoya disease, four acute ischemic stroke, three transient ischemic attacks; of these, five had unilateral internal carotid occlusion, while two had bilateral internal carotid artery occlusion. The root-mean-squared time difference between the xeCT and MRI studies was 27 h. In 11 of 20 patients (55%), xeCT was acquired before MRI.

xeCT CBF

CT was performed using a GE LightSpeed 8 detector scanner (GE Healthcare, Waukesha, WI) integrated with a stable xenon enhancer system (Diversified Diagnostic Products, Inc., Houston, TX). The xeCT protocol interrogated four contiguous slices (axial mode, slice thickness 10mm, field of view 25 cm, 80 kVp, 240 mA), beginning at the level of the basal ganglia, aligned with the superior orbitomeatal axis. Eight sets of images were acquired at 45-sec intervals, and the total time for the xeCT examination was 6 min. The first two time points were acquired while the patient breathed room air, and the remaining six time points were acquired with the patient breathing 28% xenon (Xe) gas, 20% oxygen, remainder air through a snug facemask. An end-tidal gas analyzer recorded expired Xe concentration, which was associated with the alveolar Xe concentration. The alveolar Xe concentration was assumed to correspond to the arterial Xe concentration, a reasonable approximation, except in patients with severe respiratory disease and abnormal alveolar-to-arterial gradient. CBF was calculated using the Kety-Schmidt method by the manufacturer's dedicated commercial software (Diversified Diagnostic Products, Inc.) according to Johnson et al. (18). The output was CBF maps with in-plane spatial resolution on the order of 2–3mm.

MRI

All MRI scans were performed at 1.5 T (Signa LX/i; GE Medical Systems, Waukesha, WI). Anatomic imaging was performed in addition to the perfusion measurements and always

included fluid-attenuated inversion recovery and diffusion-weighted imaging, with a *b* value of 1000 sec/mm^2.

DSC was performed using gradient-echo echo planar imaging during passage of 0.1 mmol/kg of either gadopentetate dimeglumine (Magnevist; Berlex Laboratories, Wayne, NJ) or gadodiamide (Omniscan; GE Healthcare), delivered using a power injector at 4 mL/sec. Image readout was performed using a multishot, multiecho Generalized Autocalibrating Partially Parallel Acquisitions (GRAPPA) echo planar imaging sequence with an acceleration factor of 3 and pulse repetition time/echo time of 1225/(17,30,52) ms (19). Twelve to 15 axial slices of 5mm thickness separated by 1.5mm interslice gap covered the entire supratentorial brain. In-plane resolution was 2.6mm (matrix 96 × 96, field of view 240mm). The DSC images required 2 min to acquire. Again, the slices were aligned with the superior orbitomeatal axis.

AIF and venous output function detection and deconvolution with block-circulant singular value decomposition (10) were performed, using a regularization threshold of 15% of the maximum singular value, in line with the work of Wu et al. (10), to create maps of CBF, cerebral blood volume (CBV), mean transit time, and AIF-corrected time-to-peak of the residue function (Tmax). To avoid subjective selection of AIF and venous output function, we employed automatic selection of 10 voxels each, based on location, peak value, peak width, and contrast arrival time (20). This algorithm resulted in AIF locations in middle cerebral arteries, anterior cerebral arteries, basilar artery, or internal carotid arteries. The venous output function locations were typically in the superior sagittal sinus, transverse sinus, or straight sinus.

Transverse relaxivity change (ΔR_2*) was calculated using a weighted least-squares fit of the signal intensity from the three acquired echoes (15). A nonlinear relationship between blood tracer concentration and transverse relaxivity was assumed for tissue, according to theoretical and experimental work (14,21,22). For the tissue signal, a linear relationship between the change in transverse relaxation rate, ΔR_2*, and gadolinium concentration, $c(t)$, was used:

$$c(t)=\frac{\Delta R_2 * (t)}{r^2} \quad [1]$$

where a relaxivity of $r_2 = 0.044$ (ms mM)$^{-1}$ was assumed for gadolinium at 1.5 T. For the AIF, a quadratic relationship between relaxivity and concentration was used (21):

$$\Delta R_2 * (t)=ac(t)+bc(t)^2 \quad [2]$$

where $a = 7.6 \times 10^{-3}$ (ms mM)$^{-1}$ and $b = 574 \times 10^{-6}$ (ms mM^2)$^{-1}$ for 1.5 T gradient-echo. All subsequent calculations were performed with the data expressed in these units of tracer concentration.

Pulsed continuous ASL was performed using a labeling period (*TL*) of 1500 ms, followed by a 2000-ms post-label delay (*w*) (23). Readout was accomplished with a three-dimensional background suppressed fast-spin-echo stack-of-spirals method. Multiarm spiral imaging was used, with eight arms and 512 data points acquired on each arm (bandwidth ± 62.5 kHz), yielding in-plane spatial resolution of 3mm. Forty 4mm-thick slices in the axial plane were acquired without intraslice gaps. Because the spirals are interleaved, both echo time (2.5 ms) and total readout time (4 ms) could be kept quite short, resulting in excellent performance in high-susceptibility regions. Pulse repetition time was approximately 5.5 sec. A high level of background suppression was achieved by the use of four separate inversion pulses placed after the labeling pulse during the postlabel delay period (at 1.49 sec, 0.68 sec, 0.25 sec, and 0.06

sec before readout). The sequence required 6 min to acquire, which included proton density images required for CBF quantitation. Postprocessing was performed using an automated reconstruction script that returned CBF images directly to the scanner console within 1 min. CBF (in milliliters/100 g/minute) was calculated in each voxel using the following equation:

$$CBF = 6000 \frac{\lambda(1 - \exp(-2.0s/1.2s))\exp(w/T_{1blood})}{2\alpha\, T_{1blood}(1 - \exp(-TL/T_{1blood}))} \frac{\Delta S}{S_0} \quad [3]$$

where λ is the brain:blood partition coefficient (0.9 mL/g), w is the postlabel delay (2.0 sec), T_{1blood} is the T_1 of arterial blood at 1.5 T (1.4 sec), α is the labeling efficiency (0.85), TL is the labeling duration (1.5 sec), ΔS is the ASL difference signal (i.e., label-control image), and S_0 is the proton density signal intensity. The term $(1 - \exp(-2.0s/1.2s))$ in the numerator reflects the presence of a saturation pulse that is applied in the proton-density images and allows conversion between measured MR signal (S_0) and the unperturbed longitudinal gray matter magnetization.

Combining ASL and DSC CBF Measurements

To determine an ASL-based global CF, we determined the location of all voxels with relatively rapid arterial arrival time, as measured by the DSC Tmax maps. Multiple different Tmax thresholds ($\text{Tmax}_{\text{thresh}}$) were examined, ranging from <1.5 sec to <6 sec at 0.5-sec intervals, as well as an infinite Tmax (i.e., all voxels were used for determining the CF). We found that shorter $\text{Tmax}_{\text{thresh}}$ (i.e., less than 1.5 sec) did not reliably include voxels in all patients for the subsequent calculations. While in practice it is reasonable to choose only voxels with the shortest Tmax, we examined these other conditions to evaluate the sensitivity to Tmax threshold choice and any potential tradeoffs. After three-dimensional rigid-body registration of ASL and DSC, the mean CBF calculated from only the voxels that met the Tmax criteria were calculated for both the ASL and DSC, yielding a patient-specific CF:

$$CF = \left\langle \frac{CBF_{ASL}(\mathbf{r})}{CBF_{DSC}(\mathbf{r})} \right\rangle, \text{mean of voxels } \mathbf{r} \text{ in which } Tmax <= \text{Tmax}_{\text{thresh}} \quad [4]$$

This dimensionless scaling factor was then multiplied with the DSC CBF map to determine the "corrected" hybrid ASL-DSC CBF, which we term CBF_{CAD}:

$$CBF_{CAD} = CF \times CBF_{DSC} \quad [5]$$

Figure 1 is a schematic of the steps taken during this process.

Finally, we chose to examine the performance of this method against another proposed method for converting DSC CBF maps from relative to absolute units in the literature (12,24), that of assigning an ROI of normal appearing white matter to 22 mL/100 g/min. ROIs comprising 180 voxels (1.8 mL) were manually positioned in the white matter on the superiormost slice corresponding to the centrum semiovale. DSC CBF maps were then scaled such that this ROI measured 22 mL/100 g/min. Results are presenting in Table 1.

Data Analysis

Rigid-body rotation based on mutual information using SPM5 (Wellcome Department of Imaging Neuroscience, University College of London, London, England) was used to coregister the MR and xeCT images. Typically, fluid-attenuated inversion recovery anatomic

images were coregistered to the four contiguous xeCT slices, and this transformation was then applied to the DSC and ASL CBF maps. Each slice was then divided into 1-mL cubic ROIs, using a "battleship grid" consisting of contiguous square ROIs. This yielded a large number of voxels with equal spatial resolution (about 400 voxels per patient) that were free of any possible region-of-interest (ROI) selection bias. Voxels belonging to the ventricles and cortical sulcal CSF were excluded by thresholding the diffusion-weighted images manually. In each patient, scatterplots of the individual DSC and ASL CBF maps with xeCT were created, yielding slope, intercept, and correlation coefficient (*R*).

The global mean CBF was calculated by averaging the (~400) individual ROI measurements described above in each patient. The MRI-based CBF measurements were normalized by the xeCT CBF value using the CBF ratio:

$$CBF\ ratio_x = \frac{MRI_x CBF_{mean}}{xeCT\ CBF_{mean}} \text{where } x \in (DSC, ASL, CAD) \quad [6]$$

where all values are global means. Ideally, this value should be 1, which would represent exact correspondence (i.e., no bias) between the two techniques. To determine the precision of the CBF between patients, the coefficient of variation (COV), or normalized between-patients standard deviation, was used:

$$COV = \frac{SD_{CBF\ ratio}}{mean_{CBF\ ratio}} = \frac{\sqrt{\sum_n (CBF\ ratio_n - \overline{CBF\ ratio})^2/(n-1)}}{\overline{CBF\ ratio}} \quad [7]$$

where the overbar represents the mean of all *n* patients and SD is standard deviation. Lower COV represents a more precise measurement. A COV of 0% means that each MRI-based CBF measurement corresponds to the xeCT CBF measurements to the level of a patient-independent scaling factor.

CBV was also calculated from the DSC maps before correction, using the ratio of the integrated tissue and venous output function concentration-time curve; postcorrection CBV maps were created by multiplying the precorrection DSC images by the same CF described above.

Linear regression was performed comparing the mean xeCT-based and MRI-based CBF measurements between patients.All postprocessingwas performed usingMatlab 7.3 (MathWorks Inc., Natick, MA). Stata, release 9.2 (StataCorp LLP, College Station, TX), was used for all statistical calculations. All values are reported as mean ± standard deviation. $P < 0.05$ was considered significant.

RESULTS

Figure 2 demonstrates a typical coregistered data set, including xeCT CBF, as well as the three different MRI-based approaches (DSC alone, ASL alone, and combined) in a patient with acute ischemic stroke. It can be seen that the ASL demonstrates a region of both high and low CBF in the right middle cerebral artery territory, which is not present on either the DSC or xeCT CBF maps. However, the uncorrected DSC CBF map markedly underestimates true CBF, as measured by xeCT. The CBF_{CAD} image demonstrates both improved representation of the right MCA region and improved quantitative CBF levels.

Figure 3 demonstrates the effect of varying $Tmax_{thresh}$. In short, we found that the precise threshold was not critical: within the range from 2 to 6 sec, the mean CF ranged between 2.28 ± 1.32 and 2.53 ± 1.37. Without any thresholding based on the Tmax lesions (i.e., using all colocalized voxels in the ASL and DSC scans), CF was 2.48 ± 1.32. However, the CF in individual patients varied significantly, consistent with the idea that this is a patient-specific factor; for example, using a Tmax threshold of 3 sec, the range of the CF in the different patients ranged from a low of 1.02 to a high of 6.71.

As the threshold increases, more voxels are included in each patient for the calculation of CF (Fig. 3), with about 50% of voxels included for Tmax between 3 and 4 sec. Based on the improved precision and low bias, we believe that a Tmax of 3 sec represented the best operational choice for $Tmax_{thresh}$ in this patient population. Table 1 presents the mean CBF data for xeCT, uncorrected DSC, ASL, and the combined method for a range of $Tmax_{thresh}$, including nonthresholded (i.e., $Tmax_{thresh}$ = infinity). CBF measured using the CAD approach had a bias roughly equivalent to the ASL method, but the precision of the measurement, as reflected by the COV improved, decreasing to 33% from 47% for $Tmax_{thresh}$ of 3 sec. Finally, the method in which a normal-appearing white matter ROI is set to 22 mL/100 g/min partially improves interpatient variability (COV 36%) but causes about 30% overestimation in mean CBF compared with the xenon CT gold standard (Table 1). As in the work of Mukherjee et al. (12), the reason for this is that the xenon CT CBF values in these ROIs had a wide range, from 6 mL/100 g/min to 35 mL/100 g/min. Figure 4 shows the mean CBF measurements for each MRI method compared with xeCT CBF.

In individual patients, both ASL and uncorrected DSC had similar correlation for all voxels ($R = 0.34 \pm 0.16$ for ASL, $R = 0.39 \pm 0.13$ for DSC). Multiplication of the DSC images by a global CF will not improve correlation of individual CBF ROI measurements in individual patients; however, when ROIs from all patients were combined, there was a significantly improved correlation of the CBF_{CAD} maps ($R = 0.32$ for CAD-CBF, $R = 0.30$ for ASL, $R = 0.26$ for DSC; $n = 6496$ voxels, $P < 0.05$ for all values being different from each other). This effect was particularly evident when considering only voxels with long Tmax (one example is shown as Fig. 5, for $Tmax_{thresh}$ of 3 sec, examining only voxels with Tmax >7.5 sec). In these regions, the correlation of combined maps is higher than that of the ASL CBF maps.

While we did not have a gold standard for evaluating CBV, we note that the CF above can be applied to these maps and can be compared with literature values. The mean CBV in the brain increased from 1.63 ± 0.79% (precorrection) to 3.50 ± 1.42% (postcorrection) for a $Tmax_{thresh}$ of 3 sec.

DISCUSSION

Problems With Existing ASL and DSC CBF Methods

ASL has been shown to accurately measure quantitative CBF in normal volunteers (25), but it has not been validated in a patient population with a wide variety of cerebrovascular disease and extensive collateral flow. In particular, CBF errors are known to occur in regions with prolonged arterial arrival times (4–6), which may lead to CBF under- or overestimation, depending on the precise relationship between arterial arrival time and the sequence's postlabel delay time, as well as whether vessel suppression techniques are used. This can lead to a confusing picture, and for this reason, many have doubted whether ASL could play a role in the diagnosis and management of patients with severe cerebrovascular disease, particularly acute stroke patients.

Some of these problems can be mitigated by the use of ASL sequences with multiple postlabel delay times (6,26,27). Improved estimation of CBF in the setting of variable delay can be

accomplished by nonlinear fitting of the ASL difference signal data to a generalized kinetic model or by using a "model-free" approach, in which the difference between non-vessel-suppressed and vessel- suppressed images acts as an AIF. However, this method cannot be used for regions supplied by very slow collateral pathways, in which no ASL difference signal is observed even for the longest postlabel delays. Also, multiple postlabel delay ASL sequences necessarily have either reduced SNR for individual time points or an overall increase in scan time.

DSC CBF methods yield robust *relative* CBF maps, especially if delay-invariant deconvolution methods are performed (10). However, prior studies have shown that the intersubject variability with DSC CBF measurements is significant (11,12,28,29), which has been attributed to a host of factors, including AIF partial volume, vessel orientation sensitivity, AIF clipping due to signal saturation, nonlinear contrast relaxivity, susceptibility-induced voxel location shifting, and differences in large vessel/small vessel hematocrit, such that absolute CBF quantitation is challenging in individual patients. While degradation of the AIF shape and regularization will contribute to quantitation errors, we hypothesize that the major contribution to CBF quantitation errors emanates from scaling issues due to the aforementioned effects on the AIF.

Combining DSC and ASL: The Best of Both Worlds?

Both DSC and ASL, when used in isolation, thus have difficulties measuring quantitative CBF in patients with cerebrovascular disease. However, the strength of each measurement can be leveraged using a combined ASL-DSC approach, we have termed CAD-CBF. ASL quantitation is robust in regions with normal arrival times; DSC can be used to identify precisely these voxels, using the timing information that can be obtained from Tmax maps. Thus, a patient-specific CF can be determined by equating the mean CBF obtained from each method only in voxels with Tmax below a prespecified threshold. It is important to note that the precise CF is dependent upon any corrections that have been applied to scale the DSC data (e.g., brain density factor, relaxivity and relaxation rate look-up table, and small/large vessel hematocrit (Hct) correction) and therefore would likely vary, depending on the exact implementation and postprocessing steps used calculate absolute CBF. The method is only predicated on the assumption that the relative CBF maps produced by DSC are accurate or, at minimum, are more accurate than ASL. The CF value is applied to the entire DSC CBF data set, taking advantage of the better relative CBF properties of DSC in regions with long delay times, where ASL suffers from T_1-based label decay and arterial transit artifacts (e.g., incomplete arterial bolus arrival to the capillaries).

This general approach is flexible, and a similar CF can also be derived from and applied to spin-echo DSC sequences. In fact, this may be preferable, given that gradient- echo echo planar imaging is sensitive to large blood vessels (which should not be included in the perfusion measurement as this would, in theory, lead to a "flow-through artifact") (30). ASL and spin-echo-DSC also share the characteristic of being most sensitive to perfusion at the microvascular level (31,32). This may explain the remaining small underestimation of CBF by about 10% in the combined CBF maps. The use of a patient-specific CF also obviates the need for determining the magnitude of the AIF, which is fundamentally problematic for spin-echo acquisitions. This, in turn, would enable truly quantitative measurements of both microvascular CBF and CBV (11).

We found that the specific choice of $\text{Tmax}_{\text{thresh}}$ was not critical. This may seem nonintuitive, but we believe is due to the relatively small number of voxels with long Tmax in most patients with cerebrovascular disease. Thus, we found that good results were achieved even without using a threshold (i.e., determining the CF based on all the voxels within the colocalized DSC and ASL volumes); such an approach might be feasible in most patients and could reduce computational time and errors from noise in the Tmax maps. However, we believe the current

approach is most prudent, given that the CF is likely to be sensitive to $Tmax_{thresh}$ for patients with large and/or bilateral lesions, such as those seen in moyamoya disease or carotid terminus occlusions. We believe that the optimal level for $Tmax_{thresh}$ is around 3 sec as this resulted in the lowest intersubject variability, accompanied by reasonably low bias compared with gold standard xeCT CBF. Also, at this threshold, 41.1 ± 14.3% of voxels are used in the calculation, thus minimizing issues with noise that could occur with shorter $Tmax_{thresh}$.

The combined ASL-DSC method yields a better estimate of gold-standard CBF compared with either ASL or DSC used alone. Specifically, the CAD-CBF method has a bias and precision equal to or better than that for ASL, with improved correlation in voxels with long Tmax. The correlation of all voxels in all patients was also significantly increased using the combined method, though the overall difference was slight and may not be clinically relevant. However, this improvement was more pronounced in voxels with long Tmax (see Fig. 5), as expected, given the challenges of ASL imaging in such regions. Finally, while we could not compare the corrected CBV values with a gold standard, the use of the CF did increase the mean whole-brain CBV (3.5 ± 1.4%) to the level of literature values (3.8 ± 0.7%), as measured by $C^{15}O$ Positron Emission Tomography (PET) (33).

The method does require that two perfusion studies be obtained, adding either 2 or 6 min to the protocol, depending on which sequence one considers to have added. The ASL sequence used in the current study obtains three number of averages (NEX) to increase SNR. This was done because we ask our clinicians to examine both ASL and DSC hemodynamic studies, and only one average for the ASL study results in poor image quality. However, for the purposes of measuring the CF, it is likely that fewer NEX are required since the CF is derived from mean values calculated in a large ROI (usually about half of the total imaged volume); this would lead to a reduction in imaging time and could be incorporated into a “prescan” module of the DSC measurement. For the same reason, larger voxels can be used. The added SNR affords the use of parallel imaging, which would further reduce scan time. It should be noted that differences in geometric distortion between the ASL and the DSC acquisitions could lead to imperfect registration on a voxel-by-voxel basis and could conceivably affect the CF calculation. In our implementation, the ASL is a three-dimensional spin echo sequence, while the DSC is a two-dimensional gradient echo echo planar imaging sequence. However, we believe the effects of this are relatively small, given the large number of voxels used for the CF calculation, most of which are not located in problematic regions such as the inferior frontal and temporal lobes. It may be desirable for this reason to acquire both the ASL prescan and the DSC images using a readout with similar geometric distortion profiles.

Other DSC Correction Approaches

Several previous reports have described approaches to normalize CBF measurements in individual patients, using a patient-specific CF. Lin et al. (28) described a method that derived a CF normalizing the area under the curve of the individual patient’s superior sagittal sinus, with the mean value derived from a small cohort of young normal volunteers. A similar method is also used in computed tomography perfusion (CTP). This method is predicated on the idea that (1) the measurement is accurate in normal volunteers and (2) the percentage of the cardiac output delivered to the brain is a constant, regardless of age or disease state. Using this method, they showed good correlation between CBF measured with DSC and $H_2^{15}O$ PET in five different patients with unilateral carotid occlusion. They did not report on whether the accuracy was equivalent between the affected and unaffected hemispheres, which would be expected to have markedly different transit delay times. Mukherjee et al. (12) examined a similar group of seven patients with chronic unilateral internal carotid artery occlusion. They found that the scaling the individual measurements such that a deep white matter ROI was fixed to be 22 mL/100 g/min, a value derived from PET studies, did not significantly improve the correlation of DSC

and gold-standard PET CBF measurements (data not reported). We found that the use of this method was associated with partial improvement in interpatient variability, but, like Mukherjee et al. (12), that the absolute CBF values were overestimated. In addition, this method is quite subjective and time consuming compared with the CAD-CBF approach.

Sakaie et al. (29) proposed a novel "bookend" method, in which steady-state CBV measurements obtained using T_1-weighted images before and after bolus contrast passage could be used to determine a patient-specific CF, with the assumption that there is slow exchange between intra- and extravascular water on the time scale of the measurement. They demonstrated that the use of this CF led to a reduction in the variability of CBF measurements between different normal young volunteers and that the CBF levels were more compatible with literature values, though they did not perform direct comparison with a gold-standard method. The method has the advantage of being self-calibrated, in that neither a separate gold-standard measurement nor a population-averaged mean value is required. It does require two additional sequences obtained before and after the bolus perfusion study, which added 4 min to their protocol.

Limitations

The current study is limited by several factors. First, the number of patients was relatively small. It is possible that there are CBF errors even in the ASL-derived maps in regions with short Tmax or that the specific model used to convert ASL difference signal and proton-density images into CBF values is not valid. There could be leakage of contrast on DSC images that is spatially variable, leading to errors in the final CAD-CBF maps. Also, the block-circulant singular value decomposition method used for calculation of CBF and Tmax on the DSC maps, while accounting in theory for delay, does not address relative CBF errors related to bolus dispersion or inaccurate representation of AIF shape due to clipping or partial- volume artifact.

The calculation of the CF requires that the relative CBF be comparable between the two techniques, and it should be remembered that ASL uses a diffusible tracer to measure CBF, while DSC (whether gradient echo or spin echo) is based on a nondiffusible tracer. In particular, gradientecho echo planar imaging maps that included large vessels (i.e., partial-volume contribution from arterioles and venules) could lead to systemic underestimation of the CF since the vessels tend to have short Tmax, and this may explain the persistent slight underestimation in the CAD-CBF maps compared with xeCT. Also, we chose to determine a CF based only on Tmax; one could conceive of other approaches to select the appropriate voxels, including criteria based on tissue type (gray versus white matter), baseline CBF levels, or even presence or absence of pathology. We emphasize that this is a first-level approach that is relatively easy to implement, and it is possible that other metrics could be applied that may further improve the accuracy of the technique.

Finally, the data analysis assumes that the CBF for both the MRI and xeCT sessions was equal; systemic CBF differences could occur between the examinations, and scans were not performed at the same time of day or under the same diet or CO_2 conditions. It is possible that much of the remaining variability in the measurement is due to these factors. Also, there is some evidence that the inhalation of xenon-enriched gas can lead to small (5%) CBF increases (16).

CONCLUSION

We have demonstrated a method that we have termed CAD-CBF, based on combined DSC and ASL imaging methods, which has reduced bias and precision when compared to gold-standard xeCT CBF. A patient-specific scaling factor is derived from equating the CBF levels on the ASL and DSC images only in regions with short arterial arrival times. Correlation

between CAD-CBF method and xeCT CBF is improved, particularly in regions with long arterial arrival times. We believe the approach supports the use of both ASL and DSC in patients with cerebrovascular disease. For scaling purposes, we anticipate that an ASL scan with a coarser resolution than used in this study would be sufficient. Thus, a much more time-efficient ASL method could be used that would minimize the additional time needed for this calibration measurement.

Acknowledgments

The study was partially supported by the Neuroradiology Education and Research Foundation Scholar Award (G.Z.) and the Lucas Foundation.

Grant sponsor: NIH; Grant number: R01-NS066506.

References

1. Villringer A, Rosen BR, Belliveau JW, Ackerman JL, Lauffer RB, Buxton RB, Chao Y, Wedeen VJ, Brady TJ. Dynamic imaging with lanthanide chelates in normal brain: contrast due to magnetic susceptibility effects. Magn Reson Med 1988;6:164–174. [PubMed: 3367774]
2. Dixon WT, Du LN, Faul DD, Gado M, Rossnick S. Projection angiograms of blood labelled by adiabatic fast passage. Magn Reson Med 1986;3:454–462. [PubMed: 3724425]
3. Detre JA, Leigh JS, Williams DS, Koretsky AP. Perfusion imaging. Magn Reson Med 1992;23:37–45. [PubMed: 1734182]
4. Alsop DC, Detre JA. Reduced transit time sensitivity in noninvasive magnetic resonance imaging of human cerebral blood flow. J Cereb Blood Flow Metab 1996;16:1236–1249. [PubMed: 8898697]
5. Detre JA, Samuels OB, Alsop DC, Gonzalez-At JB, Kasner SE, Raps EC. Noninvasive magnetic resonance imaging evaluation of cerebral blood flow with acetazolamide challenge in patients with cerebrovascular stenosis. J Magn Reson Imaging 1999;10:870–875. [PubMed: 10548801]
6. Hendrikse J, van Osch MJ, Rutgers DR, Bakker CJ, Kappelle LJ, Golay X, van der Grond J. Internal carotid artery occlusion assessed at pulsed arterial spin-labeling perfusion MR imaging at multiple delay times. Radiology 2004;233:899–904. [PubMed: 15486211]
7. Wolf RL, Alsop DC, McGarvey ML, Maldjian JA, Wang J, Detre JA. Susceptibility contrast and arterial spin label perfusion MRI in cerebrovascular disease. J Neuroimaging 2003;13:17–27. [PubMed: 12593127]
8. Smith AM, Grandin CB, Duprez T, Mataigne F, Cosnard G. Whole brain quantitative CBF and CBV measurements using MRI bolus tracking: comparison of methodologies. Magn Reson Med 2000;43:559–564. [PubMed: 10748431]
9. Østergaard L, Weisskoff RM, Chesler DA, Glydensted C, Rosen BR. High resolution measurement of cerebral blood flow using intravascular tracer passages, part I: mathematical approach and statistical analysis. Magn Reson Med 1996;36:715–725. [PubMed: 8916022]
10. Wu O, Ostergaard L, Weisskoff RM, Benner T, Rosen BR, Sorensen AG. Tracer arrival timing-insensitive technique for estimating flow in MR perfusion-weighted imaging using singular value decomposition with a block-circulant deconvolution matrix. Magn Reson Med 2003;50:164–174. [PubMed: 12815691]
11. Østergaard L, Johannsen P, Host-Poulsen P, Vestergaard-Poulsen P, Asboe H, Gee AD, Hansen SB, Cold GE, Gjedde A, Gyldensted C. Cerebral blood flow measurements by magnetic resonance imaging bolus tracking: comparison with [(15)O]H_2O positron emission to-mography in humans. J Cereb Blood Flow Metab 1998;18:935–940. [PubMed: 9740096]
12. Mukherjee P, Kang HC, Videen TO, McKinstry RC, Powers WJ, Derdeyn CP. Measurement of cerebral blood flow in chronic carotid occlusive disease: comparison of dynamic susceptibility contrast perfusion MR imaging with positron emission tomography. AJNR Am J Neuroradiol 2003;24:862–871. [PubMed: 12748086]
13. van Osch MJ, van der Grond J, Bakker CJ. Partial volume effects on arterial input functions: shape and amplitude distortions and their correction. J Magn Reson Imaging 2005;22:704–709. [PubMed: 16261570]

14. Kiselev VG. On the theoretical basis of perfusion measurements by dynamic susceptibility contrast MRI. Magn Reson Med 2001;46:1113–1122. [PubMed: 11746577]
15. Jochimsen TH, Newbould RD, Skare ST, Clayton DB, Albers GW, Moseley ME, Bammer R. Identifying systematic errors in quantitative dynamic-susceptibility contrast perfusion imaging by high-resolution multi-echo parallel EPI. NMR Biomed 2007;20:429–438. [PubMed: 17044140]
16. Gur D, Good WF, Wolfson SK Jr, Yonas H, Shabason L. Local cerebral blood flow measured by xenon-enhanced CT. Science 1982;215:1267–1268. [PubMed: 7058347]
17. Yonas H, Darby JM, Marks EC, Durham SR, Maxwell C. CBF measured by Xe-CT: approach to analysis and normal values. J Cereb Blood Flow Metab 1991;11:716–725. [PubMed: 1908474]
18. Johnson DW, Stringer WA, Marks MP, Yonas H, Good WF, Gur D. Stable xenon CT cerebral blood flow imaging: rationale for and role in clinical decision making. AJNR Am J Neuroradiol 1991;12:201–213. [PubMed: 1902015]
19. Newbould RD, Skare ST, Jochimsen TH, Alley MT, Moseley ME, Albers GW, Bammer R. Perfusion mapping with multiecho multishot parallel imaging EPI. Magn Reson Med 2007;58:70–81. [PubMed: 17659630]
20. Straka, M.; Mlynash, M.; Zaharchuk, G.; Albers, GW.; Bammer, R. Can a human operator be replaced by a computer for processing of bolustracking perfusion data?. Proc International Society of Magnetic Resonance in Medicine (ISMRM); Honolulu, HI. 2009; p. 1466
21. Kjolby BF, Ostergaard L, Kiselev VG. Theoretical model of intravascular paramagnetic tracers effect on tissue relaxation. Magn Reson Med 2006;56:187–197. [PubMed: 16724299]
22. van Osch MJ, Vonken EJ, Viergever MA, van der Grond J, Bakker CJ. Measuring the arterial input function with gradient echo sequences. Magn Reson Med 2003;49:1067–1076. [PubMed: 12768585]
23. Dai W, Garcia D, de Bazelaire C, Alsop DC. Continuous flow driven inversion for arterial spin labeling using pulsed radiofrequency and gradient fields. Magn Reson Med 2008;60:1488–1497. [PubMed: 19025913]
24. Østergaard L, Sorensen AG, Kwong KK, Weisskoff RM, Gyldensted C, Rosen BR. High resolution measurement of cerebral blood flow using intravascular tracer bolus passages, part II: experimental comparison and preliminary results. Magn Reson Med 1996;36:726–736. [PubMed: 8916023]
25. Ye FQ, Berman KF, Ellmore T, Esposito G, van Horn JD, Yang Y, Duyn J, Smith AM, Frank JA, Weinberger DR, McLaughlin AC. H(2)(15)O PET validation of steady-state arterial spin tagging cerebral blood flow measurements in humans. Magn Reson Med 2000;44:450–456. [PubMed: 10975898]
26. Macintosh BJ, Pattinson KT, Gallichan D, Ahmad I, Miller KL, Feinberg DA, Wise RG, Jezzard P. Measuring the effects of remifentanil on cerebral blood flow and arterial arrival time using 3D GRASE MRI with pulsed arterial spin labelling. J Cereb Blood Flow Metab 2008;28:1514–1522. [PubMed: 18506198]
27. Petersen ET, Lim T, Golay X. Model-free arterial spin labeling quantification approach for perfusion MRI. Magn Reson Med 2006;55:219–232. [PubMed: 16416430]
28. Lin W, Celik A, Derdeyn C, An H, Lee Y, Videen T, Ostergaard L, Powers WJ. Quantitative measurements of cerebral blood flow in patients with unilateral carotid artery occlusion: a PET and MR study. J Magn Reson Imaging 2001;14:659–667. [PubMed: 11747021]
29. Sakaie KE, Shin W, Curtin KR, McCarthy RM, Cashen TA, Carroll TJ. Method for improving the accuracy of quantitative cerebral perfusion imaging. J Magn Reson Imaging 2005;21:512–519. [PubMed: 15834910]
30. Buxton RB. Quantifying CBF with arterial spin labeling. J Magn Reson Imaging 2005;22:723–726. [PubMed: 16261574]
31. Boxerman JL, Hamberg LM, Rosen BR, Weisskoff RM. MR contrast due to intravascular magnetic susceptibility perturbations. Magn Reson Med 1995;34:555–566. [PubMed: 8524024]
32. Fisel CR, Ackerman JL, Buxton RB, Garrido L, Belliveau JW, Rosen BR, Brady TJ. MR contrast due to microscopically heterogeneous magnetic susceptibility: numerical simulations and applications to cerebral physiology. Magn Reson Med 1991;17:336–347. [PubMed: 2062208]
33. Ito H, Kanno I, Kato C, Sasaki T, Ishii K, Ouchi Y, Iida A, Okazawa H, Hayashida K, Tsuyuguchi N, Ishii K, Kuwabara Y, Senda M. Database of normal human cerebral blood flow, cerebral blood volume, cerebral oxygen extraction fraction and cerebral metabolic rate of oxygen measured by

positron emission tomography with ^{15}O-labelled carbon dioxide or water, carbon monoxide and oxygen: a multicentre study in Japan. Eur J Nucl Med Mol Imaging 2004;31:635–643. [PubMed: 14730405]

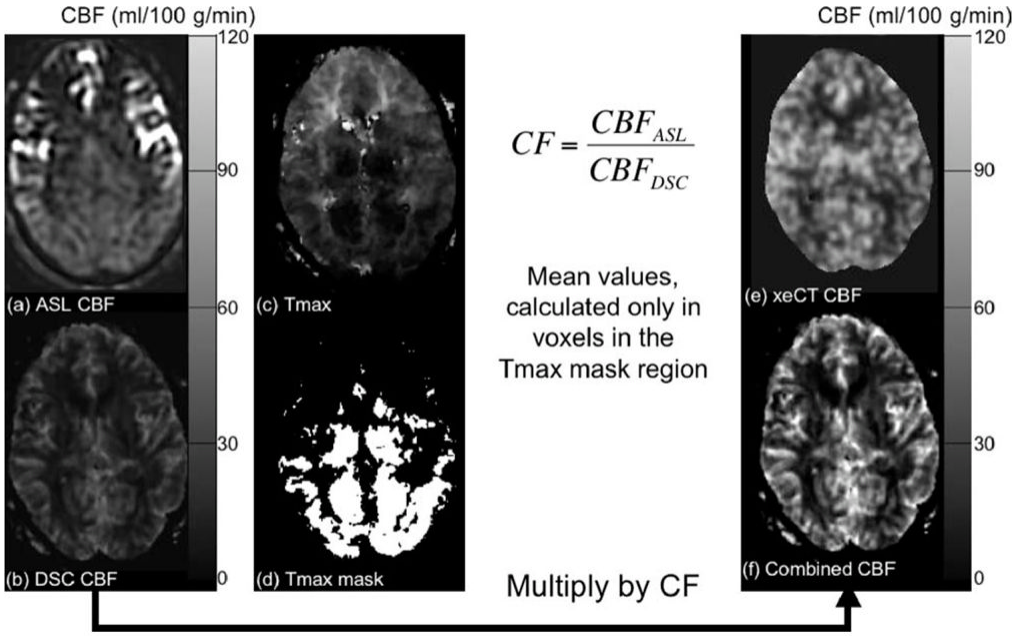

FIG. 1.

Demonstration of the method of determining the CF for combined ASL and DSC CBF maps. **a**: ASL- and (**b**) DSC-derived MRI CBF maps in a 42-year-old man with bilateral moyamoya disease. There is marked arterial transit artifact in the bilateral anterior circulation seen on the ASL CBF maps, while the posterior circulation is unaffected. Using information from the Tmax map (**c**) acquired during the DSC study, a thresholded Tmax mask (**d**) can be created to include only voxels with Tmax shorter than a prespecified threshold (in this example, $Tmax_{thresh}$ = 3 sec). The CF is the ratio of the ASL-measured CBF and the DSC-measured CBF calculated only in the Tmax masked regions. The DSC-derived CBF map is then multiplied by the CF to create the combined map (**f**), which more closely compares with the xeCT CBF map (**e**) in magnitude while more accurately depicting true CBF in the affected regions.

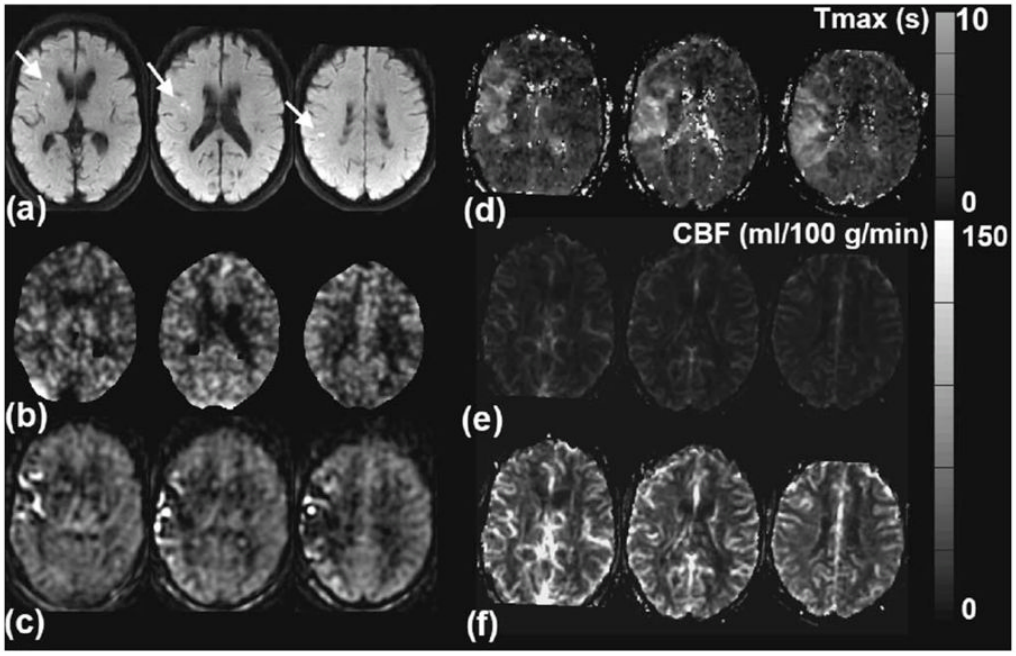

FIG. 2.

A 74-year-old man with acute onset of slurred speech and mild left facial droop. **a**: Diffusion-weighted imaging shows foci of high signal in the right middle cerebral artery territory (arrows), consistent with acute ischemic stroke. **b**: xeCT CBF map demonstrates that there is no significant CBF reduction in this region, suggesting reperfusion or adequate supply through collaterals. **c**: ASL CBF map demonstrates mixed high and low ASL signal, consistent with arterial transit artifact. CBF estimates are not accurate in the affected region. **d**: Tmax map confirms the significant delay in contrast arrival to this region. **e**: The uncorrected CBF maps derived from DSC perfusion-weighted images show no significant asymmetry but markedly underestimate xeCT CBF. On the same grayscale as the other images, this appears darker than the other images. **f**: The DSC-derived CBF maps corrected by the ASL scaling factor (using a $Tmax_{thresh}$ of 3 sec) yields the most accurate depiction of CBF, with minimal bias and correct representation of preserved CBF in the right middle cerebral artery territory. This patient did not receive thrombolysis due to the mild nature of his initial symptoms, and his infarct volume did not expand on follow-up MRI imaging (images not shown).

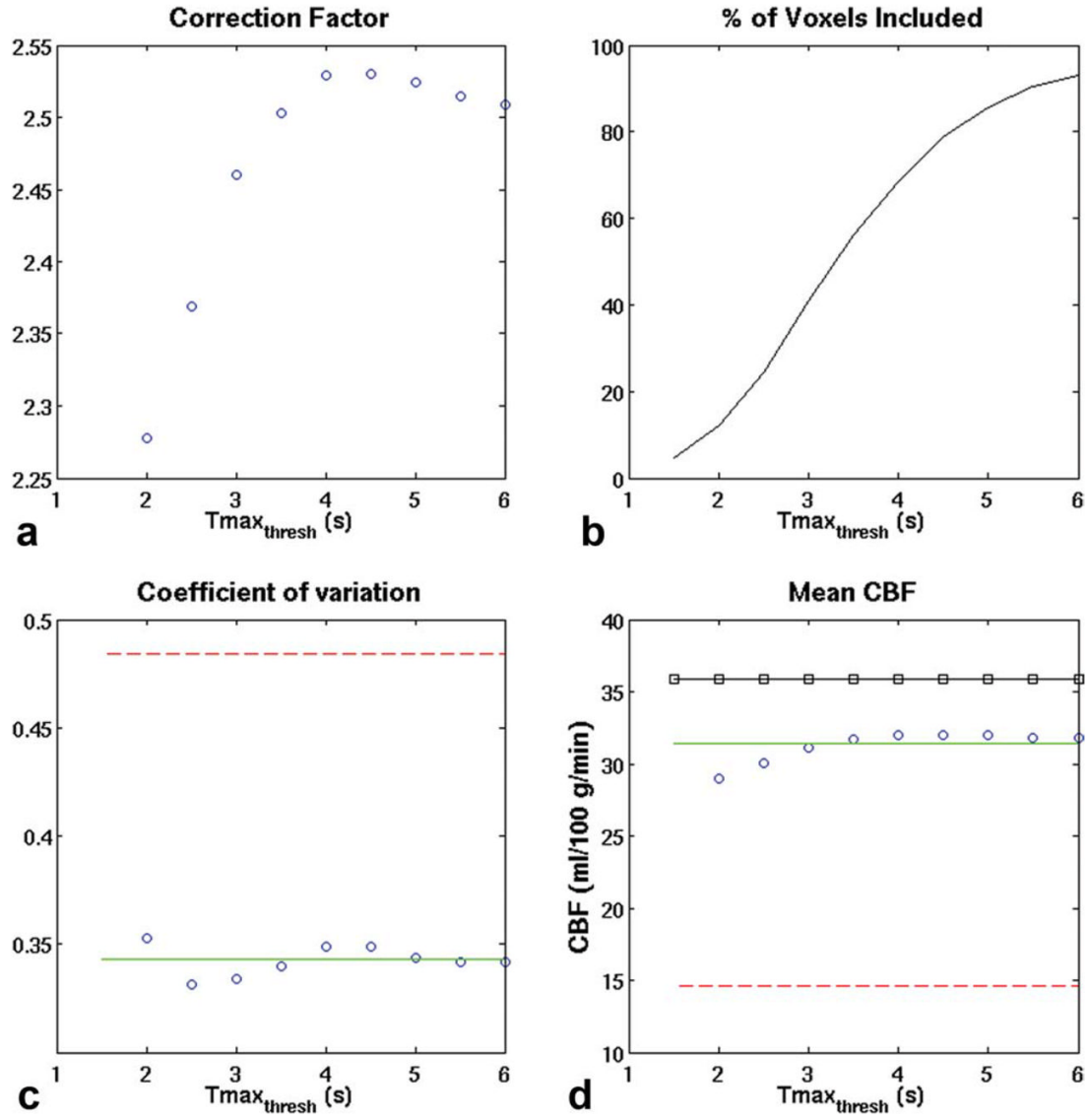

FIG. 3.

Effect of Tmax threshold on (**a**) the mean CF, (**b**) the percentage of total voxels satisfying the inclusion criteria, (**c**) the COV of the CBF ratio, and (**d**) measured CBF. Red dashed line: DSC alone. Green solid line: ASL alone. Blue circles: CAD-CBF. Black squares: xeCT CBF.

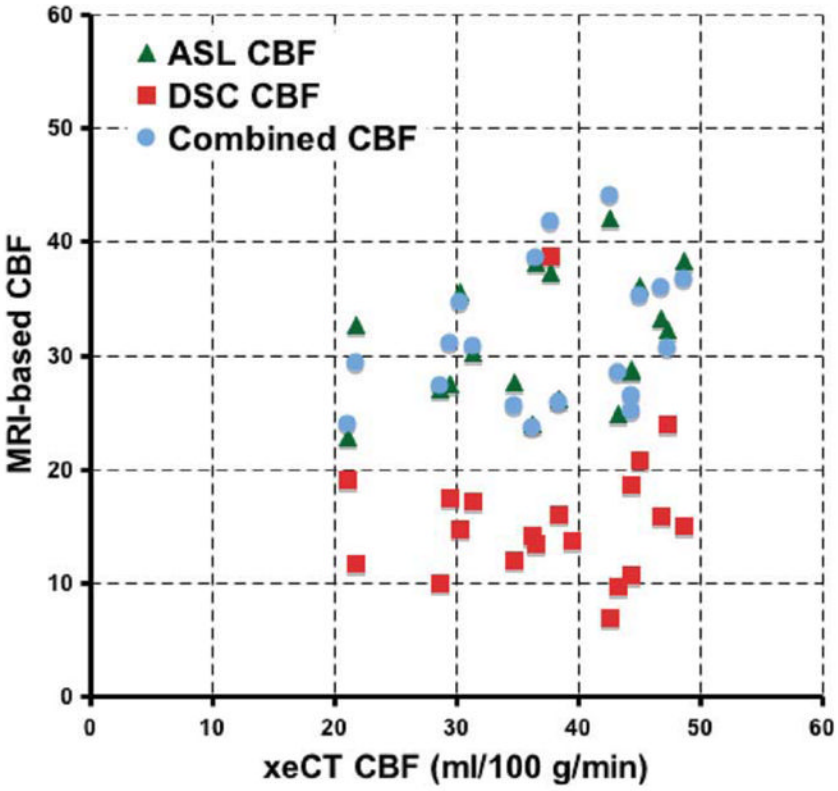

FIG. 4.

Comparison of ASL, uncorrected DSC, and CAD mean global CBF compared with gold-standard xeCT CBF. Data points shown are mean CBF values, which include all imaged tissue, and are a mixture of gray and white matter for each patient. Note the improved bias in the measurement of the ASL and CAD CBF methods compared with the uncorrected perfusion-weighted image method. The correlation of both the ASL and the CAD CBF maps was 0.23 ($P < 0.05$), while the correlation of the uncorrected DSC CBF images was 0.04 (P = non-significant). [Color figure can be viewed in the online issue, which is available at www.interscience.wiley.com.]

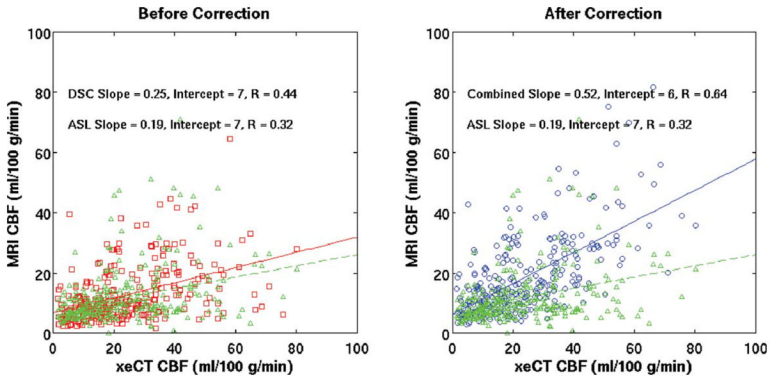

FIG. 5.

Comparison of correlation between the MRI techniques and xeCT CBF in regions with long arterial arrival delays (Tmax > = 7.5 sec) before and after ASL-based correction in all patients (n = 289 regions). $Tmax_{thresh}$ was 3 sec. Note the improved correlation of CAD-CBF (R = 0.64) over either the ASL (R = 0.32) or the DSC uncorrected (R = 0.44) method alone. Red squares = DSC-CBF (before correction). Blue circles = CAD-CBF. Green triangles = ASL-CBF (same on both plots). Overlaid lines represent the slope and intercept of the regression (DSC uncorrected = red; CAD CBF = blue; ASL-CBF = green dashed).

Table 1

CBF Measurements Using the Different Techniques (n = 20 Patients)[†]

Method	$Tmax_{thresh}$	CBF (ml/100 g/min)	CBF Ratio	COV
xeCT (gold-standard)	–	35.8 ± 7.7	–	
DSC	–	14.6 ± 6.3[*]	0.43 ± 0.21	47%
ASL	–	31.4 ± 9.9	0.91 ± 0.31	34%
CAD-CBF	2 sec	29.0 ± 10.1	0.83 ± 0.29	35%
	3 sec	31.2 ± 9.8	0.90 ± 0.30	33%
	4 sec	32.0 ± 10.1	0.93 ± 0.32	34%
	5 sec	32.0 ± 10.0	0.93 ± 0.31	33%
	6 sec	31.8 ± 10.0	0.92 ± 0.31	32%
	∞	31.4 ± 9.9	0.92 ± 0.31	32%
DSC scaled by white matter ROI of 22 mL/100 g/min		43.4 ± 7.4	1.29 ± 0.46	36%

[†]All values mean ± standard deviation. $Tmax_{thresh}$: Tmax threshold for including voxel in the calculation of the correction factor. CBF ratio = mean MR-based CBF value divided by the mean xeCT CBF value (i.e., for no bias, CBF ratio = 1.0). COV = SD normalized by the mean (for perfect precision, COV = 0%).

[*]Significantly different from xeCT CBF ($P < 0.01$, paired t test).